Diffraction in resonant electron scattering from helical macromolecules: *A*- and *B*-type DNA

Laurent Caron* and Léon Sanche

Groupe de Recherches en Sciènces des Radiations, Faculté de Médecine, Université de Sherbrooke,
Sherbrooke, Québec J1H 5N4, Canada
(Received 2 May 2004; published 29 September 2004)

We elaborate our theoretical framework to treat low-energy electron scattering from helical macromolecules. A model of simple scatterers organized into a helical structure is proposed with application to base-pair arrangements in DNA. We extend our analysis to *A*-type DNA as well as nonperiodic arrangements in *B*-type DNA. Diffraction patterns due to base-pair spacing are observed under all conditions. We discuss the role of electron diffraction in electron attachment to the bases leading to the formation of shape and core-excited resonances. The decay of such transient anions into dissociative-state channels producing DNA strand breaks is also described. We find A-type DNA to be much more sensitive to low-energy electrons than B type.

I. INTRODUCTION

Low-energy electron-molecule scattering has been studied for more than half a century and considerable advances have been made at both the theoretical and experimental level [1–4]. The energy and angular dependence of the magnitude of cross sections for elastic, inelastic, ionizing, and dissociative processes induced by the collision of an electron with a molecule have been obtained from various types of experiments. For nearly the same period of time, theories have been developed to explain the behavior of these cross sections for molecules of increasing complexity and size. Even though reasonably successful, these theories are still limited to the treatment of relatively small molecules, usually composed of no more than a dozen atoms or so [5,6]. Our theoretical description of electron-molecule scattering is still far from that needed to understand electron scattering from most biological molecules, which are much larger and more complex. Molecules like DNA, which may contain up to 10^{10} atoms, are so huge that it becomes obvious that a different approach must be developed to tackle the scattering problem.

A framework has recently been proposed by the authors [7] to describe theoretically low-energy electron (LEE) scattering from such large biomolecules, which have a helical topology. The problem was decoupled into two parts: first the electron interacts with the entire molecule and then the new wave function, defined by the atomic arrangement within the molecule, interacts at a specific site of the molecule (e.g., a basic subunit). This choice was dictated by the important contribution to the scattering cross sections arising from both resonances and electron diffraction at low energies; i.e., electron attachment requires the localization of the electron on a small subunit of the biomolecule and an electron of energy typically $5-15$ eV has a wavelength that is of the order of molecular and intermolecular distances and is thus initially delocalized. In other words, the incident electron is first

likely to undergo multiple scattering before interacting at a specific site, where it can be captured in a resonant state. This idea of decoupling the diffracted amplitude from the final local site interaction had previously been successful in describing with *R*-matrix theory the behavior of the absolute cross section for dissociative electron attachment (DEA) to small molecules embedded in a rare gas matrix [8,9]. In this case, the scattering separates into two regions: inside the *R*-matrix sphere, where the matrix elements are those of the gas phase modified by the condensed phase, and outside the sphere, where the interaction with the rare gas atoms is dominant, causing electron diffraction which modifies the vacuum electron wave function.

In this paper, we elaborate our theoretical framework to treat LEE scattering from helical macromolecules. We first address the multiple scattering problem and then examine the various parameters that influence the coupling of the diffracted wave to electron states localized on basic subunits. More specifically, we extend our analysis to the problem of LEE scattering from *A*-type DNA as well as to that of nonperiodic sequences in *B*-type DNA. The DNA molecule consists [10] of two polynucleotide antiparallel strands having the form of a right-handed helix and composed of repeated sugar-phosphate units hydrogen bonded together through the four fundamental bases, which are covalently linked to the sugar moiety of the backbone. This is illustrated in Fig. 1 for a short double-stranded segment. It consists of two sugar rings with the bases guanine and adenine, hydrogen bonded to cytosine and thymine, respectively. The bases are chemically bonded to the sugar-phosphate unit. Under dry conditions, DNA still contains on average 2.5 water molecules per base pair [11] which easily fit in the grooves of the helix; these H_2O molecules are an integral part of the DNA structure. It should also be mentioned that the negative charge on one of the oxygens of the phosphate group is counterbalanced by a cation such as Na^+. In *B*-type DNA, the crystallographic (averaged) structure resembles that of a twisted ladder with base pairs defining the rungs and the backbone providing the side support. The helical pitch, that is, the distance for a full turn of the helix, is 3.4 nm and there are 10 rungs per turn. The base pairs are relatively planar and lie perpendicular to the helix axis. In *A*-type DNA, however, the

———————
*Permanent address: Département de Physique et Regroupement Québécois sur les Matériaux de Pointe, Université de Sherbrooke, Sherbrooke, QC J1K 2R1, Canada

70 032719-1

DNA Molecule:
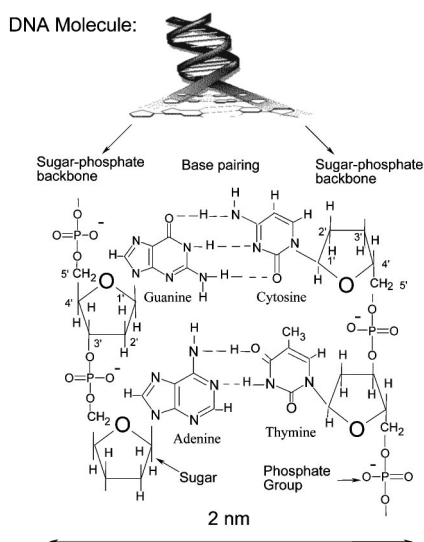
FIG. 1. Part of the *B*-type DNA structure.

vertical stacking is appreciably smaller. There are 11 residues per turn and the pitch is 2.8 nm. Moreover, there is an important tilt of 20° of the base pairs with respect to the helix axis in the *B* form.

Our interest to describe LEE interactions with DNA stems in large part from their importance for the field of radiobiology and consequent applications in radiotherapy and the environmental sciences. In fact, many of the mutagenic, genotoxic, or lethal effects of ionizing radiation can be traced to physical and chemical modifications of cellular DNA [12–14]. These lesions are induced by secondary species, generated by the primary ionizing radiation. The secondary electrons of energies below 20 eV are the most abundant of these secondary species [15,16]. About 4×10^4 secondary electrons per MeV of deposited energy are created along ionizing radiation tracks. These electrons are known to efficiently dissociate organic molecules, on subpicosecond time scales, in either the gas [2] or the condensed phase [17]. Thus, the genotoxic effects of LEEs (<20 eV) must be closely investigated in order to achieve a more complete understanding of the basic mechanisms involved in nascent radiation damage to living tissue.

Many experiments performed in the last five years now clearly demonstrate that LEE can induce considerable damage to DNA and its constituents. Available data on the fragmentation of biomolecules by LEEs have recently been reviewed [18] with emphasis on its implications for damaging DNA and its basic constituents. In recent years, technological advances have rendered possible measurements of LEE scattering and attachment processes in DNA [19–22]. It has been shown that LEEs can cause considerable damage via the dissociation of specific basic molecular units [21–26] of the DNA molecule. Such damage was found to be strongly influenced by electron resonances [19,22–26]. For example, most of the single- and double-strand breaks induced by LEEs can be related to the formation of transient anions of basic subunits of DNA (e.g., the bases and sugar analogs) and their decay into dissociative electronic states and/or DEA channel [21,25–28]. More recently, it has been possible

to demonstrate that single-strand breaks (SSBs) can be induced in DNA at energies as low as the nominal zero energy threshold ($0.1+0.3/-0.1$ eV) of the electron beam used in the experiment and that the yield as a function of energy exhibits a sharp peak at 0.8 ± 0.3 eV and a broader feature centered at 2.2 eV [29]. These features were interpreted to arise from the decay of shape resonances into the DEA channel. It was suggested that these resonances are formed by electron attachment into the empty σ^* and π^* valence molecular orbitals of the phosphate group and the DNA bases, respectively. This shape resonance mechanism is of particular importance, since it is expected to play a role not only in DNA radiolysis, but more generally in electron-DNA interactions related to the transport of charge along DNA strands, electron transfer to and from DNA, with possible applications to molecular electronics, which have generated an enormous literature. In fact, anion states created by occupation of the normally unoccupied valence molecular orbitals of a basic DNA constituent are an ingredient common to many of the processes above, albeit not always specifically recognized. In perhaps the most ephemeral example, such orbitals on bridging molecules serve to couple donor and acceptor moieties through the superexchange mechanism [30], even though the orbitals are not occupied in the normal sense.

We shall now proceed, in the next section, with the full description of the scattering model for treating electron multiple scattering in regular and irregular helical structures. We further indicate how a link can be established with resonant electron attachment. An illustrative model calculation is performed using the general topology and structure of the two forms of DNA described in this section. We then go on to discuss the implications of the results of our simulation. We end with a discussion.

II. SCATTERING MODEL

In Ref. [7], henceforth referred to as I, we presented the basic equations for electron multiple scattering in macromolecules, including DNA. For the latter, we proposed a simple model of molecular subunits (i.e., bases, sugars, and phosphates) immersed in an optical potential U_{op}, which is constant between their *R*-matrix shells (or between the muffin tins), a working hypothesis that has been used in the calculations for simple molecules [31] and in the theory of low-energy electron diffraction in solids [32]. One can quite generally describe the scattering problem of a molecular subunit by its scattering matrix $S_{LL'}$ [33,34]. Each molecular subunit has an incident plane wave of momentum $\vec{k}$ impinging on it plus the scattered waves of all other subunits. More specifically, the asymptotic form outside the *R*-matrix shell of the total wave function $\psi_{\vec{k}}^{(n)}(\vec{r})$ for a molecule centered at $\vec{R}_n$ was given by the following equation:

$$\psi_{\vec{k}}^{(n)}(\vec{r}) = 4\pi e^{i\vec{k}\cdot\vec{R}_n} \sum_{LL'} i^l B_{\vec{k}L}^{(n)} Y_{L'}(\Omega_{\vec{r}_n})$$

$$\times \left[j_l(kr_n)\delta_{LL'} + \frac{1}{2}(S_{LL'}^{(n)} - \delta_{LL'})h_{l'}^+(kr_n) \right], \quad (1)$$

where Y_L are spherical harmonics with $L=(l,m)$, j_l and $h_{l'}^+$

are the spherical Bessel function and Hankel function of the first kind, respectively, $\vec{r}_n = \vec{r} - \vec{R}_n$, and

$$B_{\vec{k}L}^{(n)} = Y_L^*(\Omega_{\vec{k}}) + \frac{1}{2} \sum_{n' \neq n L_1, L_2, L_2'} i^{l_1 + l_2 - l_2'} B_{\vec{k}L_2}^{(n')} (S_{L_2 L_2'}^{(n')} - \delta_{L_2 L_2'})$$

$$\times (-1)^{m_2'} e^{-i\vec{k}\cdot\vec{R}_{nn'}} F_{m_1, m, -m_2'}^{l_1, l, l_2'} Y_{L_1}(\Omega_{\vec{R}_{nn'}}) h_{l_1}^+(kR_{nn'}), \quad (2)$$

where

$$F_{m_1, m_2, m_3}^{l_1, l_2, l_3} = [4\pi(2l_1 + 1)(2l_2 + 1)(2l_3 + 1)]^{1/2}$$

$$\times \begin{pmatrix} l_1 & l_2 & l_3 \\ 0 & 0 & 0 \end{pmatrix} \begin{pmatrix} l_1 & l_2 & l_3 \\ m_1 & m_2 & m_3 \end{pmatrix},$$

$\begin{pmatrix} l_1 & l_2 & l_3 \\ m_1 & m_2 & m_3 \end{pmatrix}$ is the Wigner 3-j symbol [35], and $\vec{R}_{nn'} = \vec{R}_n - \vec{R}_{n'}$. Equation (2) implies a coupled set of linear equations for all $B_{\vec{k}L}^{(n)}$. As mentioned before [7], this would prove arduous if not impossible to solve were it not for the loss of coherence of the electrons due to inelastic collisions and to the presence of parasite scatterers (e.g., the structural water molecules in the grooves could be considered as such). These processes can be invoked through an imaginary part in the background optical potential U_{op} [32], i.e., an imaginary part to the electron wave number $\text{Im}(k) = \xi^{-1}$. Here ξ acts as a coherence length for the electrons. As we will show, this allows approximate though accurate *local* solutions by truncated finite-size matrices containing the information for the number of subunits within a few coherence lengths. We now wish to show how calculations can be done first for regular helical ordering and then generalize to nonregular or random situations. We then propose an application to resonant capture.

A. Regular helical structure

Let us assume the presence of a screw symmetry operation $\mathfrak{S} = \mathfrak{R}\tau$, where τ is a translation of $z_o = c/N_c$ along the helical axis $\hat{z}$ and $\mathfrak{R}$ is a rotation by an angle $\varphi_o = 2\pi/N_c$. Here N_c is the number of residues (e.g., base pairs in DNA) per turn and c is the pitch (displacement in a full turn) of the helix. One has $\mathfrak{S}\vec{R}_n \equiv \vec{R}_{\mathfrak{S}n} = z_o \hat{z} + \mathfrak{R}\vec{R}_n$. In its present form, Eq. (2) is not suitable for reduction by the screw symmetry. Let us first refine our convention for the choice of the reference axes for the spherical harmonics and the S matrix. We shall use the local reference axes $\hat{z}$, the screw axis, and $\hat{\rho}_n$, a transverse direction $(\hat{z} \cdot \hat{\rho}_n = 0)$ locked to the orientation of the nth scatterer (note that any reference direction anchored to a subunit will do). We define $Y_{lm}(\Omega^{(n)})$ to refer to the nth scatterer's reference axes. With this new convention, a change of reference implies $Y_L(\Omega^{(n')}) = Y_L(\Omega^{(n)}) e^{-im\varphi_{n'n}}$ with $\varphi_{n'n} = \arcsin[(\hat{\rho}_n \times \hat{\rho}_{n'}) \cdot \hat{z}]$. Furthermore, the invariance property of the subunits is expressed as $S_{LL'}^{(\mathfrak{S}n)} = S_{LL'}^{(n)}$. Equation (2) then becomes

$$[B_{\vec{k}L}^{(n)} - Y_L^*(\Omega_{\vec{k}}^{(n)})]e^{i\vec{k}\cdot\vec{R}_n}$$

$$= \sum_{n' \neq n} \sum_{L_1, L_2, L_2'} i^{l_1 + l_2 - l_2'} B_{\vec{k}L_2}^{(n')} (S_{L_2 L_2'}^{(n')} - \delta_{L_2 L_2'})(-1)^{m_2'} e^{i\vec{k}\cdot\vec{R}_{n'}}$$

$$\times F_{m_1, m, -m_2'}^{l_1, l, l_2'} e^{-i(m_1 + m_2')\varphi_{n'n}} Y_{L_1}(\Omega_{\vec{R}_{nn'}}^{(n)}) h_{l_1}^+(kR_{nn'}). \quad (3)$$

With this choice, one has $\Omega_{\vec{R}_{\mathfrak{S}n\mathfrak{S}n'}}^{(\mathfrak{S}n)} = \Omega_{\vec{R}_{nn'}}^{(n)}$ and $\varphi_{\mathfrak{S}n'\mathfrak{S}n} = \varphi_{n'n}$. Applying $\mathfrak{S}$ to both sides of this last equation, one gets

$$[B_{\vec{k}L}^{(\mathfrak{S}n)} - Y_L^*(\Omega_{\vec{k}}^{(\mathfrak{S}n)})]e^{i\vec{k}\cdot\vec{R}_{\mathfrak{S}n}}$$

$$= \sum_{n' \neq n} \sum_{L_1, L_2, L_2'} i^{l_1 + l_2 - l_2'} B_{\vec{k}L_2}^{(\mathfrak{S}n')} (S_{L_2 L_2'}^{(\mathfrak{S}n')} - \delta_{L_2 L_2'})$$

$$\times (-1)^{m_2'} e^{i\vec{k}\cdot\vec{R}_{\mathfrak{S}n'}} \times F_{m_1, m, -m_2'}^{l_1, l, l_2'} e^{-i(m_1 + m_2')\varphi_{\mathfrak{S}n'\mathfrak{S}n}} Y_{L_1}$$

$$\times (\Omega_{\vec{R}_{\mathfrak{S}n\mathfrak{S}n'}}^{(\mathfrak{S}n)}) h_{l_1}^+(kR_{\mathfrak{S}n\mathfrak{S}n'}). \quad (4)$$

Realizing that $\vec{k} \cdot \vec{R}_{\mathfrak{S}n} = k_z z_o + \vec{k} \cdot \mathfrak{R}\vec{R}_n = k_z z_o + \mathfrak{R}^{-1}\vec{k} \cdot \vec{R}_n$, $\Omega_{\vec{k}}^{(\mathfrak{S}n)} = \Omega_{\mathfrak{R}^{-1}\vec{k}}^{(n)}$, and $R_{\mathfrak{S}n\mathfrak{S}n'} = R_{nn'}$, one therefore has $B_{\vec{k}L}^{(\mathfrak{S}n)} = B_{\mathfrak{R}^{-1}\vec{k}L}^{(n)}$. This suggests constructing basis functions of the star of the wave vector $\vec{k}$ [36]

$$\mathfrak{B}_{pL}^{(n)} = \sum_{q=0}^{N_c - 1} e^{-ipq\varphi_o} e^{i(\mathfrak{R}^{-1})^q \vec{k} \cdot \vec{R}_n} B_{(\mathfrak{R}^{-1})^q \vec{k}L}^{(n)} \quad (5)$$

for which

$$\mathfrak{S}\mathfrak{B}_{PL}^{(n)} \equiv \mathfrak{B}_{pL}^{(\mathfrak{S}n)} = e^{i(k_z z_o + p\varphi_o)} \mathfrak{B}_{pL}^{(n)}. \quad (6)$$

These basis functions are eigenstates of the screw operator. Because of this last relation, we shall subdivide the index n into two subindices (n_z, n_b) where n_z refers to bands or slices associated with residues in the $\hat{z}$ direction of thickness z_o and $n_b = 1 \cdots N_b$ to each of the N_b scatterers within each band. Note that $\mathfrak{S}n = (n_z + 1, n_b)$. With this notation, one has the important property

$$\mathfrak{B}_{pL}^{(\mathfrak{S}n)} \equiv \mathfrak{B}_{pL}^{(n_z + 1, n_b)} = e^{i(k_z z_o + p\varphi_o)} \mathfrak{B}_{pL}^{(n_z, n_b)}, \quad (7)$$

which greatly simplifies the solution. Using this last equation in (3), one gets

$$\mathfrak{B}_{pL}^{(n_z, n_b)} = K_{pL}^{(n_z, n_b)} + \sum_{n_z', n_b' L_1, L_2, L_2'} i^{l_1 + l_2 - l_2'} \mathfrak{B}_{pL_2}^{(n_z, n_b')} e^{i(k_z z_o + p\varphi_o)(n_z' - n_z)}$$

$$\times (1 - \delta_{n_z' n_z} \delta_{n_b' n_b})(S_{L_2 L_2'}^{(n_z, n_b')} - \delta_{L_2 L_2'})(-1)^{m_2'} F_{m_1, m, -m_2'}^{l_1, l, l_2'}$$

$$\times e^{-i(m_1 + m_2')\varphi_{n'n}} Y_{L_1}(\Omega_{\vec{R}_{nn'}}^{(n_z, n_b)}) h_{l_1}^+(kR_{nn'}), \quad (8)$$

where

$$K_{pL}^{(n_z, n_b)} = \sum_{q=0}^{N_c - 1} e^{-ipq\varphi_o} e^{i(\mathfrak{R}^{-1})^q \vec{k} \cdot \vec{R}_n} Y_L^*(\Omega_{(\mathfrak{R}^{-1})^q \vec{k}}^{(n_z, n_b)}). \quad (9)$$

The number of coupled scatterers in Eq. (8) has been reduced to N_b. This is much less than in the situation using only the

Bloch theorem [36] since there are N_c more scatterers in the unit cell than in a slice.

B. Irregular helical structure

In the absence of a screw symmetry, the calculations become more tedious but still manageable essentially because of the finite coherence length ξ. One has to choose a basic structural unit or basis of length ℓ that includes a region of interest of the helix appreciably longer than ξ. This is required to ensure that the contribution to Eq. (2) coming from the edges is reduced due to phase decoherence by the factor $\approx \exp(-\ell/2\xi)$ in the central portion of the structural unit. One can then solve Eq. (2) for this isolated basis or, better yet, impose periodic boundary conditions, by choosing ℓ to be a multiple of c, and use Bloch's theorem. This has the advantage of mending the basis ends that would otherwise have been badly treated in the more direct alternative. One can then write

$$B_{kL}^{(\Upsilon n)} = e^{ik_z\ell}B_{kL}^{(n)}, \tag{10}$$

where the lattice translation Υ is defined as $\Upsilon \vec{R}_n \equiv \vec{R}_{\Upsilon n} = \vec{R}_n + \ell\hat{z}$. Equation (2) then involves only the number of molecular subunits within the basis, even though the sum over n' extends beyond it. Alternatively, if ℓ is not a multiple of the pitch length c, one can impose a screw symmetry in which τ is a translation of $z_\ell = \ell$ along the helical axis $\hat{z}$ and $\mathfrak{R}$ is a rotation by an angle $\varphi_\ell = \ell\varphi_o/z_o$ and proceed as in the previous subsection.

C. Resonant capture

In an effort to extract physically meaningful information from the multiple scattering formalism, we had targeted in I a calculation of the capture amplitude $V_{\vec{k}}^{(c)}$ of an electron in a shape resonance of a basic subunit C positioned at $\vec{R}_c$, representing one of the DNA bases. We had assumed a dominant capture channel symmetry corresponding to L_o and had used the one-center approximation of O'Malley [37] for the capture amplitude. When generalized to a multiple scattering situation, this led to

$$V_{\vec{k}}^{(c)} = \sqrt{4\pi}V_{L_o}[C_{\vec{k}L_o} + Y_{L_o}^*(\Omega_{\vec{k}})]e^{i\vec{k}\cdot\vec{R}_c}, \tag{11}$$

where

$$C_{\vec{k}L} = \sum_{n' \notin C}\sum_{L_1,L_2} i^{l_1+1}B_{kL_2}^{(n')}e^{i\delta_{n'l_2}}\sin(\delta_{n'l_2})(-1)^{m_2}e^{-i\vec{k}\cdot(\vec{R}_{cn'})}$$
$$\times F_{m_1,m,-m_2}^{l_1,l,l_2}Y_{L_1}(\Omega_{\vec{R}_{cn'}})h_{l_1}^+(kR_{cn'}) \tag{12}$$

and V_{L_o} is an energy and nuclear coordinate dependent amplitude. These equations are obtained by expanding the electronic wave function around $\vec{R}_c$.

We had not, however, extended our analysis to include the perhaps even more important process of electron attachment with core excitation. Core-excited Feshbach resonances, in particular, are expected to have sufficiently long lifetimes to

allow fragmentation. We can estimate the capture matrix element $H_{i\rightarrow j} = \langle j|H_{int}|i\rangle$ by

$$H_{i\rightarrow j} = \int\int d^3r\,d^3r'\,\varphi_\gamma^*(\vec{r})e^{i\vec{k}\cdot\vec{r}}\frac{1}{|\vec{r}-\vec{r}'|}\phi_\beta^*(\vec{r}')\phi_\alpha(\vec{r}'), \tag{13}$$

in which an electron is removed from the occupied molecular orbital $\phi_\alpha(\vec{r}')$ and added to the unoccupied $\phi_\beta^*(\vec{r}')$ orbital (the core excitation) while the incident electron, in the plane wave state $e^{i\vec{k}\cdot\vec{r}}$, winds up in the state $\varphi_\gamma^*(\vec{r})$, an unoccupied valence molecular orbital or a diffuse state such as a Rydberg state. In either case, a core-excited shape resonance can be formed when the incident electron is captured in the φ_γ state by its angular momentum barrier. With the partial wave decomposition of the plane wave, given by

$$e^{i\vec{k}\cdot\vec{r}} = 4\pi\sum_L i^l j_l(kr)Y_L^*(\hat{k})Y_L(\hat{r}), \tag{14}$$

one obtains

$$H_{i\rightarrow j} = 4\pi\sum_L i^l Y_L^*(\hat{k})H_L, \tag{15}$$

where

$$H_L = \int\int d^3r\,d^3r'\,\varphi_\gamma^*(\vec{r})j_l(kr)Y_L(\hat{r})\frac{1}{|\vec{r}-\vec{r}'|}\phi_\beta^*(\vec{r}')\phi_\alpha(\vec{r}'). \tag{16}$$

As in the case of shape resonances, i.e., Eqs. (11) and (12), one should replace $Y_L^*(\hat{k})$ in Eq. (15) by its multiple scattering generalization $[C_{\vec{k}L} + Y_L^*(\hat{k})]$. Consequently, the same fundamental combination expresses the effect of multiple scattering on the capture amplitudes of both shape and core-excited resonances. Moreover, as long as the first maximum of $j_l(kr)$ in Eq. (16), at $r = \bar{r}_l \approx \sqrt{l(l+1)}/k$, is within the outreach distance R of the molecule, the lth partial wave of the incoming electron has an important probability of presence within the molecule and the matrix element $H_{i\rightarrow j}$ will be quite substantial. There are no selection rules for the Coulomb interaction.

But when $\bar{r}_l > R$, two distinct possibilities arise. If φ_γ is contained within R, which we shall refer to as a localized core-excited resonance, then the integration over r is restricted to $r < \bar{r}_l$ and one can approximate $j_l(kr) \propto (kr)^l$. Consequently, $H_L \propto k^l$ which is a rapidly decreasing function of $k = \sqrt{2E}$ in a.u. This effectively acts as an energy cutoff at $\bar{r}_l = R$ i.e., at $E \approx l(l+1)/2R^2$ a.u. which is the same cutoff criterion used in I for shape resonances (E is the height of the centrifugal barrier needed to retain the extra electron).

However, if φ_γ is diffuse (e.g., it has a Rydberg character), one can use the spherical harmonic decomposition

$$\frac{1}{|\vec{r}-\vec{r}'|} = 4\pi\sum_{L'}\frac{r_<^{l'}}{r_>^{l'+1}}\frac{1}{(2l'+1)}Y_{L'}^*(\hat{r})Y_{L'}(\hat{r}') \tag{17}$$

in which $r_< = r'$ and $r_> = r$ for the greatest part of the integral (16) defining H_L when $r > \bar{r}_l$. One then obtains
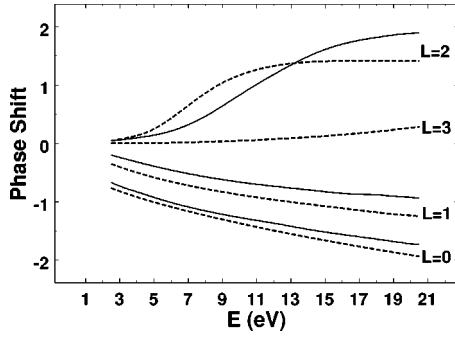
FIG. 2. Phase shifts used for Ar (full lines) and Kr (dashed lines) as a function of energy.

$$H_L \approx 4\pi \sum_{L'} C_{L'}^{\alpha\beta} \int d^3r \; \varphi_\gamma(\vec{r}) \frac{j_l(kr)}{r^{l'+1}} Y_L(\hat{r}) Y_{L'}^*(\hat{r})$$

$$\approx 4\pi \sum_{L'} \frac{C_{L'}^{\alpha\beta} D_{LL'}^\gamma}{\bar{r}_l^{l'+1}}, \tag{18}$$

where $D_{LL'}^\gamma = \int d^3r \; \varphi_\gamma(\vec{r}) j_l(kr) Y_L(\hat{r}) Y_{L'}^*(\hat{r})$ and $C_{L'}^{\alpha\beta} = \int d^3r'(r')^{l'} \phi_\beta(\vec{r}') \phi_\alpha(\vec{r}') Y_{L'}(\hat{r}')$. Here, $C_{L'}^{\alpha\beta}$ is the partial wave component of the molecular excitation. Since the molecular states are not in our situation eigenvalues of the angular momentum, there should normally be contributions from most L'. One can thus expect H_L to decrease in a milder fashion at low energy for diffuse states as compared to the previous situation when φ_γ is localized on the molecule. There is no cutoff in this situation. The electron can excite the molecule from a distance due to the long-range character of the Coulomb interaction and transit to the diffuse state.

We now propose the partial capture factor

$$\Gamma(L_o) = \left| \sqrt{4\pi} \left[C_{kL_o}^- + Y_{L_o}^*(\Omega_{\vec{k}}) \right] \right|^2 \tag{19}$$

as a meaningful measure of the effect of multiple scattering on the capture probability in the L_o channel for both types of resonances.

III. SIMULATION

Let us now illustrate these procedures by specializing our theory to a helical macromolecule made of repeating rung units (residues) of pseudomolecules (PMOLs) that are constructed from centrosymmetric scatterers. The sum over n in Eq. (2) and (8) then runs over the individual scatterers. Moreover, for single centrosymmetric scatterers, one has $1/2(S_{LL'}^{(n')} - \delta_{LL'}) = i\delta_{LL'} e^{i\delta_{nl}} \sin(\delta_{nl})$ where δ_{nl} is the nth scatterer phase shift. We have used throughout not only the phase shifts of Ar[38] as in our previous calculations, but also those of Kr to investigate the effects of a larger scatterer at certain atomic positions. These phase shifts shown in Fig. 2 were deduced from Ref. [39] by removing the polarization outside the muffin tin.

In I, we had used the following parameters: a screw pitch of $c=3.4$ nm and a number of residues per turn $N_c=10$ which
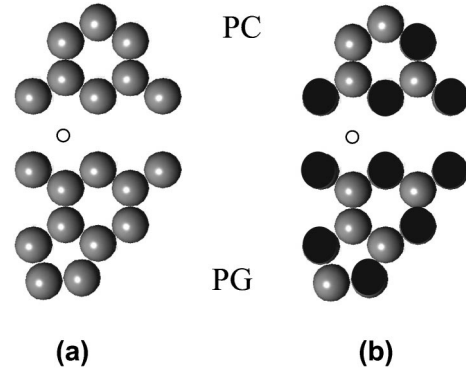

FIG. 3. The basic pseudomolecular PC-PG units used, defining a rung, are shown (a) with the phase shifts of Ar and (b) for mixed Ar-Kr phase shifts, the black circles representing Kr. The open circle marks the position of the helix's rotation axis.

are characteristic of the B form of DNA described in the Introduction, the $l=0,1,2$ phase shifts of the electronically inert species argon, and a value of the wave function coherence length of 20 Bohr radii, that is $\xi=1.06$ nm. This value is representative of solids [32,38] and biological materials [20]; furthermore, it compensated for the artificial regularity of the helix. We had constructed two PMOLs. These are PC and PG of Fig. 3 built around hexagonal rings of side-length equal to the C-C distance of benzene [6], 0.14 nm, and a distance of 0.56 nm between ring centers. This ring structure is fundamental to the structure of the DNA bases [10]. The PMOL arrangement bears resemblance to the central part of the C-G base pairing in the B-DNA decamer of Ref. [40]. Finally, we had chosen the incident direction to be perpendicular to the axis of the helix. This choice was suggested by the experiments [19,27,20,28], in which the damage to the DNA molecule is measured for electrons impinging in a direction normal to a condensed film of the molecule. In such experiments, electrons are thus incident predominantly perpendicular to the DNA strands, which are expected to lie mostly in the plane of the films.

In I, we had plotted the relative partial capture factor $\Gamma_{rel}(L_o)$ which is Γ of Eq. (19) divided by its value without multiple scattering,

$$\Gamma_{rel}(L_o) = \left| \sqrt{4\pi} \left[C_{kL_o}^- + Y_{L_o}^*(\Omega_{\vec{k}}) \right] \right|^2 \Big/ \left| \sqrt{4\pi} Y_{L_o}^*(\Omega_{\vec{k}}) \right|^2. \tag{20}$$

for various values of L_o. Unfortunately, there was an encoding error of Eq. (8), which originated from the many phase factors in this expression. As a consequence, the calculations were incorrect. They overemphasized the axial redistribution of the scattered electrons, which led us to conclude a sizable increase of capture cross sections in axial channels (small $|m_o|$). Here, we have redone the calculations of I. The results of I for the Ar scatterer arrangement of Fig. 3(a) and for $m_o = l_o$ are not considerably modified for $l_o > 1$ as can be seen in Fig. 4), i.e., there is little change in the capture probability due to multiple scattering. However, the additional results for $l_o = 0, 1$ show a different trend. There is an appreciable enhancement for these channels. Note that the $l_o = 0$ curve cor-
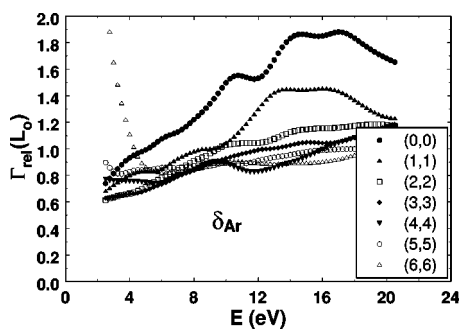
FIG. 4. Relative partial capture factor, Eq. (20), at the center of the PC ring as a function of electron energy relative to $\mathrm{Re}(U_{op})$ using Ar phase shifts. Various even symmetry entrance channels $L_o = (l_o, l_o)$ are shown.

FIG. 6. Partial capture factor at the center of the PC ring as a function of electron energy relative to $\mathrm{Re}(U_{op})$ using Ar phase shifts and for various values of the number of base pairs in a screw pitch. The values of Γ_{rel} for $L_o = (0,0)$ and of Γ for $L_o = (1,0)$ were selected.

responds to the square of the absolute value of the wave function at $\vec{R}_c$ for an incident plane wave of unit amplitude.

We resort to a plot of Γ for those axial channels $l_o + m_o = $ odd having a node in the plane of the PMOLs, since $Y_{L_o}^*(\Omega_{\vec{k}}) = 0$ for them. The incident electron, being of even parity with respect to the z component of the wave function, does not couple to odd parity channels. This quantity serves as a measure of the axial redistribution of scattered electrons and does so in a more sensitive and direct way than in I. Its value is zero for isolated PMOLs. As shown in Fig. 5, some of the very important enhancements for axial channels reported in I have now been shifted to lower energies, in a range that is not physically important for shape resonances or localized core-excited resonances. In this case, the threshold energy for capture $E_o = l_o(l_o + 1)/(2R^2)$ a.u. is to be evaluated at the outreach distance $R \approx 5$ a.u, typical of the benzene ring [5]. One obtains $E_o \sim 1, \sim 3, \sim 6, \sim 11, \sim 16, \sim 22$ eV relative to $\mathrm{Re}(U_{op})$ for $l_o = 1, 2, 3, 4, 5, 6$. Thus, the strong rise in magnitude of the partial waves (4,1), (5,0), and (6,1) with decreasing energy falls in an energy range only accessible to diffuse core-excited resonances. However, the strong maxima in the other partial waves are physically significant for all resonances.

It is interesting to note that the odd parity signals of Fig. 5 are present because of the helical structure. On one hand, they would be absent in a macromolecule having vertical
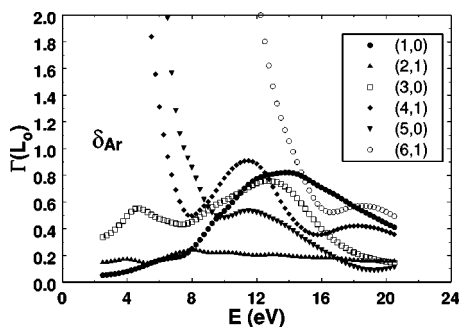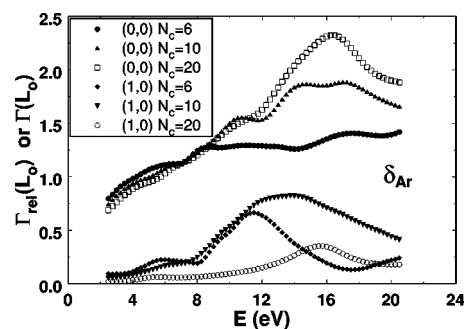
alignment of the base pairs because the base-pair planes then have mirror symmetry. On the other hand, if the twist angle φ_o is too large, the axial overlap decreases and the interference along the helix axis direction is weakened. We have studied different twist angle situations by varying N_c, while keeping the inter-rung (inter-base-pair) distance z_o constant. The results of this calculation are shown in Fig. 6. It is quite clear that as N_c increases and the base-pair overlap increases, so does $\Gamma(0,0)$. *It is also seen that* $\Gamma(1,0)$ *has an absolute maximum at* $N_c = 10$, *the value of the B form of DNA.* These same channels bear the clear signature of axial diffraction. It is easily seen in Figs. 7 and 8 that as the inter-rung distance increases from $0.8z_o$ to $1.2z_o$, the maxima in both the $(0,0)$ and $(1,0)$ channels shift to lower energies.

In view of a suspected sensitivity to the phases in Eq. (8), we thought of modifying our PMOLs as shown in Fig. 3(b), by using the phase shifts of Kr to represent N or O atoms. The results, which are to be compared to Figs. 4 and 5, are shown in Figs. 9 and 10. Aside from more aggressive behavior below 12 eV due to the Kr phase shifts and the ensuing effect on multiple scattering within base pairs, the quantitative behavior is quite similar. This is reassuring, indicating that our model provides trends in the magnitude of the capture cross sections, which are not too sensitive to the phase shifts of the atoms of the DNA bases, although the details of the energy dependence may be different.
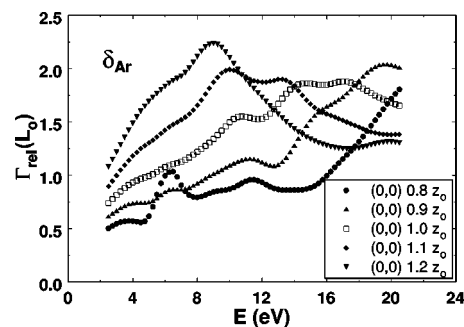

FIG. 5. Partial capture factor, Eq. (19), at the center of the PC ring as a function of electron energy relative to $\mathrm{Re}(U_{op})$ using Ar phase shifts. Various odd symmetry entrance channels $L_o = (l_o, m_o)$ are shown.

FIG. 7. $L_o = (0,0)$ relative partial capture factor at the center of the PC ring as a function of electron energy relative to $\mathrm{Re}(U_{op})$ using Ar phase shifts and for various values of the inter-base-pair distance. z_o represents the crystallographic inter-base-pair distance.
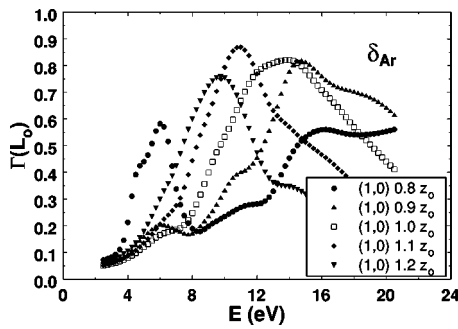
FIG. 8. $L_o = (1,0)$ partial capture factor at the center of the PC ring as a function of electron energy relative to Re(U_{op}) using Ar phase shifts and for various values of the inter-base-pair distance. z_o represents the crystallographic inter-base-pair distance.

We have also done a calculation for an irregular structure by building a basis of ten base pairs chosen at random between four possible arrangements: those of Figs. 3(b) and 11, along with their reflections on the horizontal line passing through the helix axis position. This simulates variations in base-pair relative slide and sequencing. With a coherence length of 20 a.u., roughly three base-pair distances z_o, a unit cell having the pitch length $10z_o$ is quite long and the end effects should not be too important. In any case, this is just to illustrate the use of Eq. (2) for an irregular helix. As can be seen in Fig. 12, the diffraction signature in the $(1,0)$ channel is still quite visible. It is mostly the lower-energy region $E \lesssim 12$ eV of the $(0,0)$ channel that is affected. In this energy range, the multiple scattering, which normally amplifies the base-pair scattering patterns as in Fig. 9, is less efficient. The PMOL's imprint has thus been attenuated by the disorder. As mentioned in Sec. II when introducing Im(k), disorder is akin to loss of coherence.

Finally, we have considered the A form of DNA. The phase shifts of Ar and the PMOL arrangement of Fig. 3(a) were used in this calculation. Whereas the B form only breaks the z axis mirror symmetry by the twisting of the helix, the base pairs of the A form, described in the Introduction, are known to have a substantial tilt angle of 20°. This leads to additional symmetry breaking. Moreover, the base-pair packing is much more compact due to the smaller pitch $c = 2.8$ nm and a larger number of residues per turn $N_c = 11$.
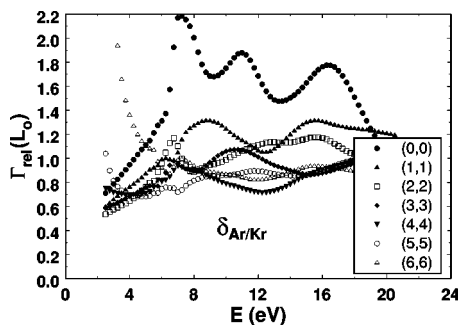

FIG. 9. Relative partial capture factor at the center of the PC ring as a function of electron energy relative to Re(U_{op}) using Ar and Kr phase shifts. Various one-center entrance channels (l_o, l_o) are shown.
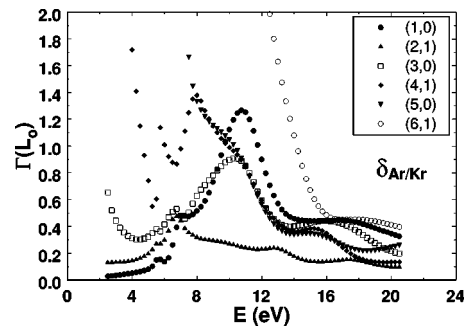

FIG. 10. Partial capture factor at the center of the PC ring as a function of electron energy relative to Re(U_{op}) using Ar and Kr phase shifts. Various odd symmetry one-center entrance channels $L_o =$ are shown.

One might expect considerable differences in multiple scattering interferences. As is seen in Figs. 13 and 14, the result is spectacular for the odd symmetry channels. The even symmetry channels show the PMOL imprint for energies less than 12 eV. Such a signature was also observed, although at a reduced level, in Figs. 9 and 10. Note that the diffraction peaks have been pushed to higher energy, outside the plotted energy range.

The large increase of $\Gamma(L_o)$ as the energy decreases, which is observed throughout our simulations, comes from the rapid rise of the Hankel function $h_{l_o}^+(kR)$ [see Eq. (12)] with decreasing kR, which is more pronounced at larger l_o. The smaller inter-base-pair distance z_o of the A form of DNA is at the origin of the larger values relative to those of the B form.

IV. DISCUSSION

We have studied the effect of diffraction in the $(0,0)$ and $(1,0)$ partial waves in the B-form helical structures and found it to be quite robust to changes in the scatterers and to disorder. The diffraction pattern is observed in many odd and even channels: $(0,0)$, $(1,0)$, $(3,0)$, and even $(4,1)$. This remains so even in presence of disorder (results not shown here). It should be emphasized that disorder is the rule rather
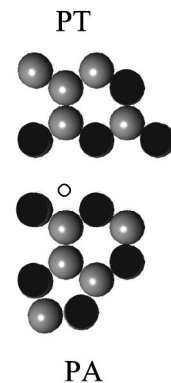

FIG. 11. The basic pseudomolecular PT-PA unit for mixed Ar-Kr phase shifts, the black circles representing Kr. The open circle marks the position of the helix's rotation axis.
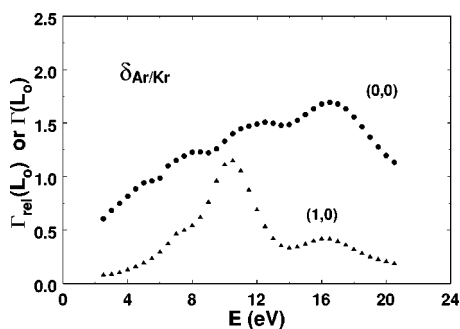
FIG. 12. Base-pair averaged partial capture factor at the center of the PC and PT rings as a function of electron energy relative to $Re(U_{op})$. The values of Γ_{rel} for $L_o=(0,0)$ and of Γ for $L_o=(1,0)$ were selected. The phase shifts of Ar and Kr were used in a random arrangement of base pairs.

FIG. 14. Partial capture factor at the center of the PC ring of the A form of DNA as a function of electron energy relative to $Re(U_{op})$ using Ar phase shifts. Various odd symmetry one-center entrance channels $L_o=(l_o,m_o)$ are shown.

than the exception in DNA [10]. We have only simulated the irregular base-pair sequencing typical of the genes. There are also local variations in the inter-base-pair distance and the twist angle. This angle is sensitive to the environment. In solution, for instance, the twist angle is reduced by 4%. There is as well the occurrence of roll of the base pairs, bending of the helix, and dynamic disorder. It is thus important to be able to treat disorder of all kinds. Our proposed approach can do this.

Curiously, the peak in the odd symmetry channels has a height that seems to be optimal for the particular twist angle of B-form DNA. We do not know if there is a particular significance to this finding.

In I, we had discussed the peak in strand breaks of DNA around 10 eV in the light of what we had thought to be a large enhancement in the shape resonance capture channels at that energy. Our findings here are more modest for these resonances but still indicate that large enhancements are possible in the case of core-excited resonances. Due to their longer lifetimes, these are likely to be responsible for the strong peaks observed in the yields of DNA strand breaks [19,22] induced by LEEs. There is, however, some uncertainty in the energy of the diffraction peaks between even and odd symmetry situations, relative to $Re(U_{op})$, which puts them in the 12–16 eV range. To bring them down in coincidence with the 10 eV double-strand breaking peak would
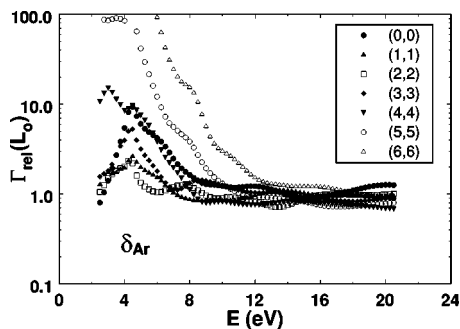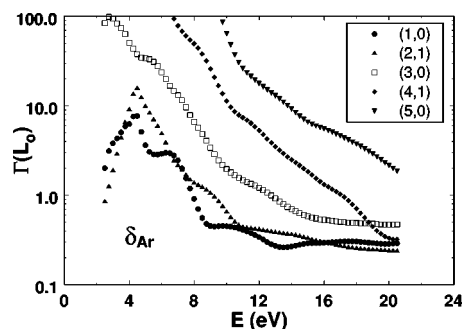
require -6 eV $\lesssim Re(U_{op}) \lesssim -2$ eV, which is not unreasonable. In this case, the energy thresholds E_o of the last section, relative to vacuum, would be shifted by some -2 to -6 eV. Therefore, those channels for which $l \lesssim 4$ might contribute to shape or localized core excitation resonant capture around 10 eV relative to vacuum. All channels, however, will contribute in diffuse core-excited resonances with substantial enhancement possibilities for the large L_o values. It is interesting to note that the energies at which diffraction effects are most prominent lie within the range where most secondary electrons are created in irradiated biological media [15,16]. We find here that, at least for the partial waves for which diffraction effects are important, the cross section for DNA damage by secondary electrons should be enhanced due to diffraction.

As mentioned in the Introduction, at much lower energies (0–4 eV), there are also shape resonances which lead to strand breaking [29]. It has been proposed [41] that such low-energy shape resonances may be formed on the bases. The anion thus formed would act as intermediary to sugar-phosphate C-O bond breaking via electron transfer. In their electron transmission experiments, Aflatooni *et al.* [42] do indeed resolve many π^* resonances in the 0.5–4.0 eV range for the DNA bases in the gas phase. Our simulations indicate no important enhancement in this range for B-DNA with respect to the single-molecule scattering situation. There is even a slight reduction due to multiple scattering. The situation is, however, quite different for the A form which shows considerable enhancement.

The very special situation observed for the helical structure of the A form suggests that it is very fragile to damage by electrons of low energy. Our data indicate that there might be an enhancement of the resonant capture cross sections by a factor of up to 10 at $E\sim10$ eV relative to vacuum, i.e., 12 to 16 eV relative to $Re(U_{op})$) for the $(3,0)$ and $(4,1)$ channels in Fig. 14 and for the $(3,1)$ channel (data not shown). Similarly, around 5 eV relative to $Re(U_{op})$) or 0 to 3 eV relative to vacuum, the enhancement could also be as large as 10 for the $(0,0)$, $(1,0)$, $(2,0)$ (data not shown), $(3,0)$, and $(2,1)$ channels, but only of 2 for the $(1,1)$ and $(2,2)$ channels.

FIG. 13. Relative partial capture factor at the center of the PC ring of the A form of DNA as a function of electron energy relative to $Re(U_{op})$ using Ar phase shifts. Various one-center entrance channels $L_o=(l_o,l_o)$ are shown.

V. CONCLUSIONS

We have treated the problem of resonance electron scattering from large biomolecules having a helical topology. We first considered the diffraction of the electron wave within the molecule followed by a calculation of the electron capture probability at a specific site within the target. By investigating electron scattering from the helical arrangement of the bases within the A and B forms of DNA, we reached a number of conclusions regarding the effects of diffraction on the magnitude of electron waves inside the molecule and on resonant electron capture processes.

Due to diffraction, the partial waves of the incoming electron wave function are considerably modified. As a result, the capture probability at a basic subunit of the macromolecule can be quite different from that for the same subunit isolated in space (i.e., in the gas phase). Intramolecular diffraction not only modifies the amplitudes of the incoming partial waves, but also introduces strong oscillations in these amplitudes as a function of electron energy. One should therefore be careful in interpreting the results of electron scattering experiments from such large molecules. In this case, maxima in inelastic scattering cross sections, which are often automatically attributed to the formation of transient anions, could arise from destructive or constructive interference of dominant partial waves inside the macromolecule. As shown in this work, for DNA the magnitude and energy of these interferences not only depend on the degree of ordering of the bases, but it is also influenced by other geometrical characteristics including inter-base-pair distance and base twist and tilt angle. This has been clearly demonstrated by showing the large differences, between A and B forms of DNA, in the diffracted partial wave content. Of course, the scattering matrix elements for a specific subunit also influence the magnitude and energy dependence of the scattered amplitudes or of a given fragmentation process.

Understanding the differences in electron scattering from the A and B forms of DNA may be of particular importance within the context of low-energy electron impact experiments, which so far have been performed under ultrahigh vacuum (UHV) on thin DNA films deposited on a metal substrate [18–22,29]. In these experiments, B-type DNA in solution is lyophilized on the metal substrate, which is then placed in an UHV chamber. Under such high vacuum, DNA loses its water shell and only structural H_2O remains bonded at specific sites inside the molecule [11]. This water reduction is expected to shrink DNA to its A form [10] so that, although the topology of DNA has not been measured in electron-impact experiments, it is possible that the electrons were actually impinging on A-type DNA. According to the present calculations, this would explain the high efficiency of 0–4 eV electrons to break a single strand of DNA [29]. Our treatment is well adapted to compare with experiments, since we chose electrons to impinge on DNA at normal incidence. We note, however, that low-energy secondary electrons are created along radiation tracks with a more isotropic distribution. Thus, in a treatment more closely related to radiobiology, the incident electron waves should be chosen as those produced by photoemission in a biological medium (e.g., water).[1]

Although the present theoretical framework was applied only to DNA, it would be possible to treat other biologically important macromolecules, such as proteins, with this formalism. Proteins are formed of long polypeptide chains composed of a sequence of amino acids. These chains, referred to as secondary structures, can have two configurations, one extended and the other helically coiled [43]. Thus, our formalism should also be applicable to electron scattering from the α-helix secondary structure of proteins whose topology exhibits a periodic helical configuration. In the case of proteins containing only an α-helix secondary structure [44], one could envisage solving the scattering problem for the entire molecule.

---

[1]Within the Born approximation, fast charged particles interact with matter by virtual emission of electromagnetic radiation; see Ref. [3].

[1] M. Allan, J. Electron Spectrosc. Relat. Phenom. **48**, 219 (1989).

[2] *Electron-Molecule Interactions and Their Applications*, edited by L. G. Christophorou (Academic, Orlando, FL, 1984), Vols. 1 and 2.

[3] I. Shimamura and K. Takayanagi, *Electron-Molecule Collision* (Plenum, New York, 1984).

[4] H. Hotop, M.-W. Ruf, M. Allan, and I. I. Fabrikant, Adv. At., Mol., Opt. Phys. **49**, 85 (2003).

[5] F. A. Gianturco and R. R. Lucchese, J. Chem. Phys. **108**, 6144 (1998).

[6] M. H. F. Bettega, C. Winstead, and V. McKoy, J. Chem. Phys. **112**, 8806 (2000).

[7] L. G. Caron and L. Sanche, Phys. Rev. Lett. **91**, 113201 (2003).

[8] I. I. Fabrikant, K. Nagesha, R. Wilde, and L. Sanche, Phys. Rev. B **56**, R5725 (1997).

[9] K. Nagesha, I. I. Fabrikant, and L. Sanche, J. Chem. Phys. **114**, 4934 (2001).

[10] R. L. P. Adams, J. T. Knowler, and D. P. Leader, *The Biochemistry of the Nucleic Acids*, 10th ed. (Chapman and Hall, New York, 1981).

[11] S. Swarts, M. Sevilla, D. Becker, C. Tokar, and K. Wheeler, Radiat. Res. **129**, 333 (1992).

[12] C. von Sonntag, *The Chemical Basis of Radiation Biology* (Taylor and Francis, London, 1987).

[13] O. Yamamoto, in *Aging, Carcinogenesis and Radiation Biology*, edited by K. Smith (Plenum, New York, 1976), p. 165.

[14] *Radiation Damage in DNA: Structure/Function Relationships at Early Times*, edited by A. Fuciarelli and J. Zimbrick (Batelle, Columbus, OH, 1995).

[15] S. Pimblott and J. LaVerne, in *Radiation Damage in DNA: Structure/Function Relationships at Early Times* (Ref. [14]), Chap. 1.

[16] V. Cobut, Y. Frongillo, J. Patau, T. Goulet, M.-J. Fraser, and J.-P. Jay-Gerin, Radiat. Phys. Chem. **51**, 229 (1998).

[17] A. Bass and L. Sanche, Radiat. Environ. Biophys. **37**, 243 (1998), a review paper.

[18] L. Sanche, Mass Spectrom. Rev. **21**, 349 (2002).

[19] B. Boudaïffa, P. Cloutier, D. Hunting, M. A. Huels, and L. Sanche, Science **287**, 1658 (2000).

[20] B. Boudaïfa, P. Cloutier, D. Hunting, M. A. Huels, and L. Sanche, Radiat. Res. **157**, 227 (2002).

[21] X. Pan, P. Cloutier, D. Hunting, and L. Sanche, Phys. Rev. Lett. **90**, 208102 (2003).

[22] M. A. Huels, B. Boudaïfa, P. Cloutier, D. Hunting, and L. Sanche, J. Am. Chem. Soc. **125**, 4467 (2003).

[23] P.-C. Dugal, H. Abdoul-Carime, and L. Sanche, J. Phys. Chem. B **104**, 5610 (2000).

[24] H. Abdoul-Carime, P. C. Dugal, and L. Sanche, Surf. Sci. **451**, 102 (2000).

[25] D. Antic, L. Parenteau, and L. Sanche, J. Phys. Chem. B **104**, 4711 (2000).

[26] H. Abdoul-Carime, P. Cloutier, and L. Sanche, Radiat. Res. **155**, 625 (2001).

[27] H. Abdoul-Carime and L. Sanche, Radiat. Res. **156**, 151 (2001).

[28] H. Abdoul-Carime and L. Sanche, Int. J. Radiat. Biol. **78**, 89 (2002).

[29] F. Martin, P. D. Burrow, Z. Cai, P. Cloutier, D. Hunting, and L. Sanche (unpublished).

[30] P. W. Anderson, in *Magnetism*, edited by G. T. Rado and H. Suhl (Academic,New York, 1963), Vol. I, Chap. 2.

[31] D. Dill and J. L. Dehmer, J. Chem. Phys. **61**, 692 (1974).

[32] J. B. Pendry, *Low Energy Electron Diffraction* (Academic, London, 1974).

[33] N. F. Mott and H. S. W. Massey, *The Theory of Atomic Collisions*, 3rd ed. (Clarendon, Oxford, 1965).

[34] F. A. Gianturco and A. Jain, Phys. Rep. **143**, 347 (1986).

[35] A. Messiah, *Quantum Mechanics* (Wiley, New York, 1962), Appendix C.

[36] M. Tinkham, *Group Theory and Quantum Mechanics* (McGraw-Hill, New York, 1964).

[37] T. F. O'Malley and H. S. Taylor, Phys. Rev. **176**, 207 (1968).

[38] M. Michaud, L. Sanche, C. Gaubert, and R. Baudoing, Surf. Sci. **205**, 447 (1988).

[39] R. P. McEachran and A. D. Stauffer, J. Phys. B **17**, 2507 (1984).

[40] G. G. Privé, K. Yanagi, and R. E. Dickerson, J. Mol. Biol. **217**, 177 (1991).

[41] R. Barrios, P. Skurski, and J. Simons, J. Phys. Chem. B **106**, 7991 (2002).

[42] K. Aflatooni, G. A. Gallup, and P. D. Burrow, J. Phys. Chem. **102**, 6205 (1998).

[43] A. Lehninger, *Biochemistry* (Worth, New York, 1970).

[44] A. Evdokimov, J. Phan, J. Tropea, K. Routzahn, H. Peters, M. Pokross, and D. Waugh, Nat. Struct. Biol. **10**, 789 (2003).